Impact of finite-size effects on computed transport properties a molecular dynamics study of dilute systems

Hulikal Chakrapani, Thejas; Hajibeygi, Hadi; Moultos, Othonas A.; Vlugt, Thijs J.H.

DOI
10.1080/00268976.2025.2578408

Publication date
2025

Document Version
Final published version

Published in
Molecular Physics

Citation (APA)
Hulikal Chakrapani, T., Hajibeygi, H., Moultos, O. A., & Vlugt, T. J. H. (2025). Impact of finite-size effects on computed transport properties: a molecular dynamics study of dilute systems. *Molecular Physics*, *123*(21-22), Article e2578408. https://doi.org/10.1080/00268976.2025.2578408

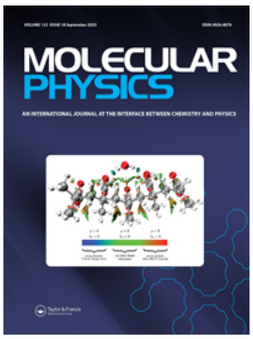

Taylor & Francis
Taylor & Francis Group

Molecular Physics

An International Journal at the Interface Between Chemistry and Physics

ISSN: 0026-8976 (Print) 1362-3028 (Online) Journal homepage: www.tandfonline.com/journals/tmph20

Impact of finite-size effects on computed transport properties: a molecular dynamics study of dilute systems

Thejas Hulikal Chakrapani, Hadi Hajibeygi, Othonas A. Moultos & Thijs J. H. Vlugt

To cite this article: Thejas Hulikal Chakrapani, Hadi Hajibeygi, Othonas A. Moultos & Thijs J. H. Vlugt (04 Nov 2025): Impact of finite-size effects on computed transport properties: a molecular dynamics study of dilute systems, Molecular Physics, DOI: 10.1080/00268976.2025.2578408

To link to this article: https://doi.org/10.1080/00268976.2025.2578408

MOLECULAR PHYSICS e2578408
https://doi.org/10.1080/00268976.2025.2578408

Taylor & Francis
Taylor & Francis Group

THERMODYNAMICS 2024 CONFERENCE (BY INVITATION ONLY)

Impact of finite-size effects on computed transport properties: a molecular dynamics study of dilute systems

Thejas Hulikal Chakrapani [a], Hadi Hajibeygi [b], Othonas A. Moultos [c] and Thijs J. H. Vlugt [c]

[a]Institute for Multiscale Thermofluids, School of Engineering, University of Edinburgh, Edinburgh, United Kingdom; [b]Reservoir Engineering, Geoscience and Engineering Department, Faculty of Civil Engineering and Geosciences, Delft University of Technology, Delft, The Netherlands; [c]Engineering Thermodynamics, Process & Energy Department, Faculty of Mechanical Engineering, Delft University of Technology, Delft, The Netherlands

ABSTRACT

Finite-size effects of transport properties computed from molecular dynamics simulations are investigated for Weeks-Chandler-Andersen systems at reduced densities of 0.05 (dilute gas), 0.45 (dense gas), and 0.85 (fluid close to the solid-liquid transition). Viscosities, self-diffusivities, Onsager coefficients, and electrical conductivities are computed for various system sizes ranging from 64 to 8192 WCA particles at each density. At dilute and intermediate densities, finite-size corrections to the transport properties significantly deviate from the widely used Yeh–Hummer correction, which was originally developed for the liquid phase.

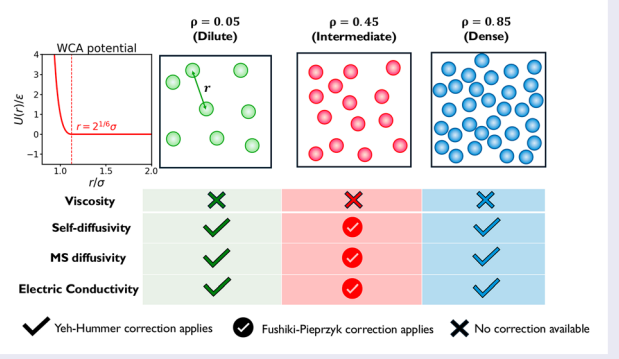

ARTICLE HISTORY
Received 3 June 2025
Accepted 6 October 2025

KEYWORDS
Finite-size effects; dilute phase; molecular dynamics; transport properties

1. Introduction

Transport properties of fluids such as bulk and shear viscosities, self- and mutual diffusivities, and electrical and thermal conductivities, are governed by the transport of momentum, mass, and energy at the molecular scale [1], respectively. Accurate prediction of these properties is critical for a wide range of applications, such as flow through porous media [2], subsurface gas storage [3], and biomedical engineering [4].

Molecular Dynamics (MD) simulations are widely used to predict transport properties of fluids [5–7]. Advances in force field development and algorithmic efficiency have enabled accurate predictions for both simple and complex fluids [5–7]. A well-known challenge in such predictions is the finite-size effect, where computed transported properties depend on the size of the simulation box, often quantified by the inverse of the length of the simulation box. This artefact arises from long-range hydrodynamic interactions that propagate across periodic boundaries. This phenomenon was first explained by Dünweg and Kremer for polymer solutions [8]. Building on this work, Yeh and Hummer (YH) derived a correction for the self-diffusivity of a solute in a single-component liquid, and validated it for SPC/E water and Lennard-Jones fluids at a reduced density of 0.7 [9]. The YH correction shows that self-diffusivities obey a linear scaling with respect to the inverse of the length simulation box. The prefactor of this finite-size term is a function of temperature and viscosity. Jamali and co-workers extended the ideas by Yeh and Hummer to mutual

CONTACT Thijs J. H. Vlugt t.j.h.vlugt@tudelft.nl

diffusivities in binary and ternary mixtures, proposing finite-size corrections for both Maxwell–Stefan (MS) [10] and Fick diffusivities [11]. The Yeh-Hummer correction is based on the observation that although self-diffusivities vary with the length of the simulation box, the liquid viscosity remains essentially independent of it. A comprehensive review of finite-size effects for diffusivities is provided by Celebi et al. [12].

Hulikal Chakrapani et al. [13] investigated transport properties of hydrogen-carbon dioxide mixtures between 5 and 50 MPa and 323.15 and 423.15 K. These authors observed that for an equimolar mixture at 50 MPa and 323.15 K, the computed viscosity still varies with the size of the simulation box. This behaviour is not usually observed in liquids. Previously, using MD simulations of WCA particles [5, 14], Kim et al. [15] have also shown that viscosity scales linearly with the inverse box length at a reduced density of 0.45, where the fluid is still expected to behave as a liquid. In sharp contrast, at a reduced density of 0.85, Kim et al. [15] showed that the liquid has a size-independent viscosity. Heyes et al. [16] conducted simulations for hard-sphere gases for various packing fractions and fit their simulation data to an analytical expression resembling the YH correction. In the limit of liquid-like densities, the expression of Heyes et al. [16] converged to the YH form, whereas significant deviations were observed at lower (gas-like) densities. These studies collectively indicate that at low densities and intermediate densities where fluids behave like dense gases, finite-size effects of computed transport properties deviate from the YH correction and must be treated with caution. Despite the studies by Kim et al. [15] and Heyes et al. [16], important gaps remain. Kim et al. [15] did not examine finite-size effects of self-diffusivities in their WCA systems, and Heyes et al. [16] did not investigate finite-size effects of viscosity. To the best of our knowledge, no prior studies have explored the finite-size effects of MS diffusivities in gases or gas mixtures. These gaps form the motivation for the present work.

In this study, we use MD simulations to investigate the finite-size effects on viscosities, self-diffusivities, and Onsager coefficients using WCA particles, i.e. a shifted Lennard-Jones potential with the attractive tail cut off [14], chosen for its computational efficiency. To compute Onsager coefficients, we use colour mixtures of WCA particles, in which particles are grouped solely for post-processing purposes while all particles interact identically with each other. Onsager coefficients are reported instead of MS diffusivities, as the former can be directly combined to obtain multicomponent MS diffusivities. Simulations are performed at three representative (reduced) densities: (a) a low-density regime ($\rho = 0.05$), where the system behaves like a dilute gas; (b) an intermediate-density regime, mimicking a dense gas ($\rho = 0.45$); and (c) a high-density regime, characteristic of liquid-like behaviour close to the solid-liquid transition point ($\rho = 0.85$) [15]. To investigate finite-size effects, we perform simulations with particle numbers ranging from 64 to 8192 in most cases. In Section 2 we elaborate on the methods adopted in our study. Section 3 contains a discussion of the finite-size effects of the transport properties for the three chosen densities before concluding in Section 4.

2. Methods

2.1. MD simulations

Viscosities, self-diffusivities, and Onsager coefficients were obtained from equilibrium molecular-dynamics (MD) simulations of Weeks–Chandler–Andersen (WCA) particles [5, 6, 14]. All particles interact via three-dimensional periodic boundaries. Throughout, we use Lennard-Jones reduced units, i.e. σ, ε, m, and k_B are set to unity [5] and all quantities are reported in reduced units, see Table 1. The Lennard-Jones pair potential is truncated and shifted at $r_c = 2^{1/6} \approx 1.122$, so that both the potential and its first derivative vanish at the cut-off. Three reduced number densities were studied, $\rho = 0.05$ (dilute), 0.45 (intermediate), and 0.85 (dense). For each density, cubic boxes containing $N = 64, 128, 256, 512, 1024, 2048, 4096$, or 8192 particles were simulated to quantify finite-size effects. The equations of motion were integrated with the leap-frog Verlet algorithm [5, 6, 17] using a reduced time step of $\Delta t = 10^{-3}$ and a fixed target temperature of $T = 1$. Simulations were performed with an in-house code.

Particles were initially placed randomly inside the box, and velocities were drawn from a Maxwell–Boltzmann distribution corresponding to $T = 1$. Each system was equilibrated for $t = 50$ in the isokinetic (NVT) ensemble [6], which strictly maintains the desired kinetic temperature. Afterwards, we switched to the microcanonical (NVE) ensemble, discarded a further $t = 50$ (5×10^5 MD steps) for additional relaxation, and then recorded pressure and particle trajectories for transport property calculations. Production runs lasted $t = 10^6$ (10^9 MD steps). Between 100 and 400 statistically independent trajectories were run for each system size, each one starting from random particle positions and velocities. The dilute state ($\rho = 0.05$) required the largest replica count to reach the target precision. Specifically, computing the Onsager coefficients at $\rho = 0.05$ required 3000 replicates, far more than were needed at the other two densities. Following Ref. [5], we divide all data for a given reduced density into five blocks. The reported mean is the average of

Table 1. Reduced (Lennard–Jones) units adopted in this work. The characteristic Lennard–Jones parameters σ, ε, and particle mass m are set to unity. The elementary charge e is also set to unity. For clarity, starred quantities $(\cdot^*)$ retain their physical units, whereas the unstarred versions are expressed in dimensionless form. The fundamental dimensions M (mass), L (length), T (time), I (current) form the basis for expressing the dimensionality of every physical quantity investigated in this study.

Quantity	Dimensional form	Reduced definition
Mass	M	$m = m^*/m$
Box Length	L	$L = L^*/\sigma$
Time	T	$t = t^*/\tau, \tau = \sigma\sqrt{m/\varepsilon}$
Charge	IT	$q = q^*/e$
Position	L	$r = r^*/\sigma$
Total Energy	ML^2T^{-2}	$E = E^*/\varepsilon$
Temperature	ML^2T^{-2}	$T = k_BT^*/\varepsilon$
Density	L^{-3}	$\rho = \rho^*\sigma^3 = N\sigma^3/V$
Pressure	$ML^{-1}T^{-2}$	$P = P^*\sigma^3/\varepsilon$
Self-diffusivity	L^2T^{-1}	$D^{\text{self}} = D^{\text{self}*}/(\sigma\sqrt{\varepsilon/m})$
Onsager coefficient	L^2T^{-1}	$\Lambda = \Lambda^*/(\sigma\sqrt{\varepsilon/m})$
MS-diffusivity	L^2T^{-1}	$D^{\text{MS}} = D^{\text{MS}*}/(\sigma\sqrt{\varepsilon/m})$
Viscosity	$ML^{-1}T^{-1}$	$\eta = \eta^*\sigma/\sqrt{m\varepsilon}$
Kinematic Viscosity	L^2T^{-1}	$\nu = \nu^*/(\sigma\sqrt{\varepsilon/m})$
Electrical conductivity	$M^{-1}L^{-3}T^3I^2$	$\kappa = \kappa^*/(e^2\sigma^{-2}/\sqrt{m\varepsilon})$

these blocks, and the uncertainty is the standard deviation of the block averages.

All transport coefficients are computed in the constant energy ensemble (*NVE*). Switching directly from the isokinetic ensemble to the *NVE* ensemble can leave the system with a total energy that produces a kinetic temperature slightly different from the target $T = 1$. To remove this bias, we carried out three short, independent $NVT \rightarrow NVE$ simulations, recorded the total energy as a function of the kinetic temperature and fitted a straight line to this. The fit reveals the total energy that would yield exactly $T = 1$. Before each production run, we keep all particle positions unchanged and scale the velocities uniformly so that the system starts the production phase with this target total energy. The method preserves the equilibrated structure at the end of the isokinetic phase while ensuring the desired total energy from the first time step onward in the production run. Using this procedure the temperatures of all our simulations were within one percent of $T = 1$.

2.2. Viscosities

We compute the shear viscosity from the Green–Kubo (GK) integral of the stress–stress autocorrelation function, following Maginn et al. [7, 18]:

$$\eta_{\text{MD}} = \frac{V}{10k_{\text{B}}T}\sum_i\sum_j\int_0^\infty \left\langle P_{ij}^{\text{os}}(t)P_{ij}^{\text{os}}(0)\right\rangle \mathrm{d}t, \qquad (1)$$

where the traceless, symmetric part of the microscopic stress tensor equals [7, 18]

$$P_{ij}^{\text{os}} = \frac{P_{ij}+P_{ji}}{2} - \left(\frac{\delta_{ij}}{3}\sum_k P_{kk}\right), \qquad (2)$$

where P_{ij} is an element of the stress-tensor [5, 6] and δ_{ij} is the Kronecker delta. The prefactor 10 accounts for the three diagonal (4/3 each) and six off-diagonal (1 each) tensor components. To improve statistics, we average the correlation over many time origins, indicated by the brackets $\langle\cdots\rangle$ in Equation (1). The time series is accumulated on-the-fly with the multiple-τ algorithm of Ramírez et al. [19], which stores far fewer data than the fixed-interval method of Frenkel and Smit [5]. This reduction is crucial for the dilute state ($\rho = 0.05$), where stress correlations decay slowly. The running integral of Equation (1) is fitted to two models recommended by Maginn et al. [7],

$$f_1(t) = A\left[\alpha\tau_1\left(1-e^{-t/\tau_1}\right) + (1-\alpha)\tau_2\left(1-e^{-t/\tau_2}\right)\right], \qquad (3)$$

$$f_2(t) = \eta_0\left[1-\exp\left[-(t/\tau_s)^{\beta_s}\right]\right], \qquad (4)$$

where the viscosity is obtained from the plateau values $A[\alpha\tau_1 + (1-\alpha)\tau_2]$ and η_0, respectively. The running integral is fitted to the two fit functions in the range $0 \leq t \leq 600$ for all systems investigated in this study. The viscosities obtained from the two fit functions differed by less than 1%, in all cases.

2.3. Self-diffusivities

Self-diffusion describes the mass transfer process driven by Brownian motion and therefore occurs even when no gradients of chemical potential, temperature, or pressure are present in the fluid [5]. For each system size, we obtain the self-diffusion coefficient from the mean-square displacement (MSD) of all particles [5, 6]:

$$D_{\text{MD}}^{\text{self}} = \lim_{t\to\infty}\frac{1}{6Nt}\left\langle\sum_{i=1}^{N}(\mathbf{r}_i(t)-\mathbf{r}_i(0))^2\right\rangle, \qquad (5)$$

where t is the correlation time, N the number of particles, and $\mathbf{r}_i(t)$ the position of particle i at time t. The factor 6 accounts for the three spatial dimensions. MSDs are accumulated on-the-fly with the multiple-τ correlator of Ramírez et al. [19]. At short times, the motion is ballistic (MSD $\propto t^2$), whereas at long times it is diffusive (MSD $\propto t$). To extract $D_{\text{MD}}^{\text{self}}$, we plot log(MSD) versus log t and choose the time window whose slope lies between 0.995 and 1.005 (within 0.5% of unity). We further ensure that inside this time window, the particle travels at least two to three box lengths. The selected time

Table 2. Time windows $[t_{\min}, t_{\max}]$ chosen for the linear (diffusive) region of the mean-square-displacement (MSD) curves. Windows were selected so that the log–log slope of MSD(t) lies within $\pm 0.5\%$ of unity.

	Self-diffusivity		MS-diffusivity	
ρ	$t_{\min}$	$t_{\max}$	$t_{\min}$	$t_{\max}$
0.05	1500	1750	1000	1250
0.45	1500	1750	100	250
0.85	1500	1750	50	200

windows for every ρ are summarised in Table 2. We use the YH correction that compensates for finite-size effects in MD-computed self-diffusivities [9],

$$D^{\text{self}} = D^{\text{self}}_{\text{MD}} + \frac{\xi k_B T}{6\pi \eta L}, \tag{6}$$

where $\xi = 2.837297$ is the lattice-sum constant for a cubic box and L is the box length. In the original YH equation, the viscosity η is assumed size-independent. Later, we will show that η can vary with L, especially at low densities, and we discuss corrections that account for this effect. The YH expression has been validated for many molecules and mixtures over a wide range of conditions [9, 20, 21]. Busch and Paschek further reduced finite-size effects by using non-cubic simulation cells [22]. For a comprehensive review of finite-size corrections to $D^{\text{self}}_{\text{MD}}$, see Ref. [12].

The YH correction rests on continuum hydrodynamics and therefore works best for dense liquids [9, 12]. At lower densities this assumption weakens, and the standard term may over- or under-correct the diffusivity. To address the issue, Fushiki [23] introduced a density-dependent factor K_H, later validated for hard spheres by Pieprzyk et al. [24]. The modified YH relation is [24],

$$D^{\text{self}} = D^{\text{self}}_{\text{MD}} + K_H \frac{\xi k_B T}{6\pi \eta L} = D^{\text{self}}_{\text{MD}} + \frac{\nu}{\nu + D^{\text{self}}} \frac{\xi k_B T}{6\pi \eta L}, \tag{7}$$

where $\nu = \eta/\rho$ is the kinematic viscosity. Piepryzk et al. [24] showed using MD simulations of hard-spheres that the factor $K_H = \nu/(\nu + D^{\text{self}})$ approaches unity in dense fluids and tends toward zero in the dilute limit, reflecting the gradual breakdown of hydrodynamic behaviour. For hard-sphere systems, this correction remains reliable down to a reduced density of about 0.2 [24]. For a reduced density below 0.2, to the best of our knowledge, there are no models to correct finite-size effects. Note that the kinematic viscosity is defined using the shear viscosity in the thermodynamic limit, η. Later, we will show that using η_{MD} instead of η hardly affects finite-size corrections to $D^{\text{self}}_{\text{MD}}$.

2.4. Onsager coefficients and Maxwell–Stefan (MS) diffusivity

Self-diffusion measures the random motion of individual molecules, whereas MS diffusivity characterises the collective mass transport of different species [25, 26] in a mixture. In MD simulations, the MS diffusivity of a binary mixture with $N = N_A + N_B$ particles of types A and B is calculated from its Onsager coefficients $\Lambda_{\alpha\beta}$ ($\alpha, \beta \in \{A, B\}$) [10, 12, 27, 28]. The Onsager coefficients for an AB binary mixture are related to the cross-correlations of particle displacements as [10, 12, 27, 28],

$$\Lambda_{AA} = \lim_{t\to\infty} \frac{\mathrm{d}}{\mathrm{d}t} \frac{1}{6N} \left\langle \sum_{i=1}^{N_A} \sum_{j=1}^{N_A} [\mathbf{r}_i(t) - \mathbf{r}_i(0)] \cdot \left[\mathbf{r}_j(t) - \mathbf{r}_j(0)\right] \right\rangle, \tag{8}$$

$$\Lambda_{AB} = \lim_{t\to\infty} \frac{\mathrm{d}}{\mathrm{d}t} \frac{1}{6N} \left\langle \sum_{i=1}^{N_A} \sum_{j=1}^{N_B} [\mathbf{r}_i(t) - \mathbf{r}_i(0)] \cdot \left[\mathbf{r}_j(t) - \mathbf{r}_j(0)\right] \right\rangle, \tag{9}$$

$$\Lambda_{BB} = \lim_{t\to\infty} \frac{\mathrm{d}}{\mathrm{d}t} \frac{1}{6N} \left\langle \sum_{i=1}^{N_B} \sum_{j=1}^{N_B} [\mathbf{r}_i(t) - \mathbf{r}_i(0)] \cdot \left[\mathbf{r}_j(t) - \mathbf{r}_j(0)\right] \right\rangle. \tag{10}$$

In our colour-mixture setup, all particles interact through the same WCA potential, while being merely tagged as type A or B so that Equations (8)–(10) can be evaluated. For such a symmetric mixture, the Onsager coefficients satisfy [10]

$$\Lambda_{AA} = \Lambda_{BB} \equiv \Lambda, \quad \Lambda_{AB} = -\Lambda. \tag{11}$$

The MS diffusivity of a general binary mixture is [10, 12]

$$D^{\text{MS}}_{\text{MD}} = \frac{x_B}{x_A}\Lambda_{AA} + \frac{x_A}{x_B}\Lambda_{BB} - 2\Lambda_{AB}, \tag{12}$$

with mole fractions $x_A = N_A/N$ and $x_B = N_B/N$. For a colour mixture, Equation (12) reduces to

$$D^{\text{MS}}_{\text{MD}} = \frac{\Lambda}{x_A x_B}. \tag{13}$$

Jamali et al. [10] derived a YH-like correction to mitigate finite-size effects of MS diffusion coefficients using

$$D^{\text{MS}} = D^{\text{MS}}_{\text{MD}} + \frac{1}{\Gamma} \frac{\xi k_B T}{6\pi \eta L}, \tag{14}$$

Table 3. Simulated colour mixtures (types *A* and *B*) used for evaluating Onsager coefficients. Each density ρ was studied at the indicated mole-fraction ratios and at all system sizes listed in the footnote.

ρ	$x_A = \frac{1}{64}$	$\frac{1}{32}$	$\frac{1}{8}$	$\frac{1}{4}$	$\frac{1}{2}$
0.85	64–8192[a]	64–8192[a]	64–8192[a]	64–8192[a]	64–8192[a]
0.45	64–4096[a]	64–4096[a]	64–4096[a]	64–4096[a]	64–4096[a]
0.05	64–1024[a]	64–1024[a]	64–1024[a]	64–1024[a]	64–1024[a]

[a]System sizes: 64, 128, 256, 512, 1024, 2048, 4096, 8192.

where D^{MS} is the finite-size corrected MS diffusivity and the second term on the right hand side is a correction term identical to Equation (6) [9] except for Γ, which is the thermodynamic factor for diffusion [25, 29]. The thermodynamic factor for diffusion reflects the non-ideality of the mixture [25, 29]. For the WCA colour mixture used in our study, Γ equals 1 by definition, which reduces the correction term to a standard YH correction for the MD computed self-diffusivities. Note that our colour mixtures are ideal diffusion mixtures and thus the MS diffusivities follow the Darken equation [10, 30, 31],

$$D^{\mathrm{MS}} = x_A D_A^{\mathrm{self}} + x_B D_B^{\mathrm{self}} = D^{\mathrm{self}}. \tag{15}$$

where $D_A^{\mathrm{self}} = D_B^{\mathrm{self}} = D^{\mathrm{self}}$. The displacement cross-correlations are accumulated on-the-fly with the multiple-τ algorithm of Ramırez et al. [19]. To locate the diffusive regime, we plot log(MSD) as a function of log t and select the time window where the slope lies between 0.995 and 1.005 (±0.5% around unity). The corresponding windows for each reduced density are listed in Table 2. Details of the simulated state points (densities, compositions, and system sizes) used for the Onsager analysis are summarised in Table 3. Table 2 shows that at $\rho = 0.05$, the lower bound t_{min} is much larger because infrequent collisions delay the onset of diffusive behaviour.

2.5. Electrical conductivities

Because the Onsager coefficients are already available, we can obtain the electrical conductivity with minimal extra effort. In this work, we evaluate the conductivity of an *AB* molten salt (no solvent) by assigning colour charges $q_A = +1$ and $q_B = -1$ and considering a charge neutral mixture ($x_A = 0.5$). The particle dynamics are unaffected by the charges which are only applied during post-processing. Following Blázquez et al. [32], the electrical conductivity is

$$\kappa = \frac{e^2\rho}{6k_BT}\left(\sum_{i=1}^{N_A}\sum_{j=1}^{N_B} q_i q_j \Lambda_{ij}\right), \tag{16}$$

with Λ_{ij} the Onsager coefficient and e is the elementary charge. For the chosen charges ($q_i = q_A = +1$, $q_j = q_B = -1$) Equation (16) simplifies to

$$\kappa = \frac{e^2\rho}{6k_BT}\left(\Lambda_{AA} + \Lambda_{BB} - 2\Lambda_{AB}\right). \tag{17}$$

Using the symmetry relations of Equation (11), we obtain

$$\kappa = \frac{4e^2\rho}{6k_BT}\Lambda. \tag{18}$$

Habibi et al. [33] showed that finite-size corrections for the electrical conductivity κ are known only for dilute salt solutions, where the standard YH expression applies. For concentrated systems such corrections are not available a priori. Below we derive the appropriate form for our molten salt. We substitute $D_{\mathrm{MD}}^{\mathrm{MS}}$ from Equation (13) evaluated at $x_A = 0.5$ into Equation (14) which yields,

$$\Lambda = \Lambda_{\mathrm{MD}} + \frac{1}{\Gamma}\frac{\xi k_BT}{24\pi\eta L}. \tag{19}$$

Λ from Equation (19) when inserted into Equation (18) yields,

$$\kappa = \frac{4e^2\rho}{6k_BT}\left(\Lambda_{\mathrm{MD}} + \frac{1}{\Gamma}\frac{\xi k_BT}{24\pi\eta L}\right), \tag{20}$$

and, after regrouping terms and substituting $\Gamma = 1$ for a colour mixture,

$$\kappa = \kappa_{\mathrm{MD}} + \frac{1}{36}\frac{\xi e^2\rho}{\pi\eta L}, \tag{21}$$

where $\kappa_{\mathrm{MD}} = \frac{4e^2\rho\Lambda_{\mathrm{MD}}}{6k_BT}$ is the electrical conductivity obtained from the Onsager coefficient Λ_{MD} computed by MD. Finally, anticipating the non-hydrodynamic nature of dilute systems the standard YH correction term in Equation (21) can be modified for dilute systems using the Fushiki [23]/Piepryzk [24] correction term

$$\kappa = \kappa_{\mathrm{MD}} + \frac{K_H}{36}\frac{\xi e^2\rho}{\pi\eta L}, \tag{22}$$

where $K_H = \frac{\nu}{\nu + D^{\mathrm{self}}}$. For the present colour mixture, by definition $\Gamma = 1$. For real molten salts, however, $\Gamma \neq 1$ and must be retained in the finite-size correction.

A summary table for the finite-size corrections of the self-, MS diffusivities and the electrical conductivities are shown in Table 4.

3. Results and discussion

3.1. Viscosities

The finite-size behaviour of the shear viscosities at the three reduced densities, $\rho = 0.85$, 0.45, and 0.05, are

Table 4. Summary of finite-size correction equations for self-diffusivity (D^{self}), Maxwell–Stefan diffusivity (D^{MS}), and electrical conductivity (κ). Here, $D^{\text{self}}_{\text{MD}}$, $D^{\text{MS}}_{\text{MD}}$, and κ_{MD} denote uncorrected MD values; η is the shear viscosity, L the box length, ρ the number density, K_H the hydrodynamic factor, ν the kinematic viscosity, and $\xi = 2.837297$ [9]. Abbreviations: Fushiki–Pieprzyk (FP) and Yeh–Hummer (YH).

Correction Type (with context)	Equation
YH for D^{self}	
(Hydrodynamic finite-size correction [8, 9])	$D^{\text{self}} = D^{\text{self}}_{\text{MD}} + \frac{\xi k_B T}{6\pi\eta L}$
FP for D^{self}	
(Generalization of YH for reduced hydrodynamic effects [23, 24].)	$D^{\text{self}} = D^{\text{self}}_{\text{MD}} + K_H \frac{\xi k_B T}{6\pi\eta L}$
YH-like for D^{MS}	
(Extension of YH to Maxwell–Stefan diffusivity [10].)	$D^{\text{MS}} = D^{\text{MS}}_{\text{MD}} + \frac{1}{\Gamma}\frac{\xi k_B T}{6\pi\eta L}$
FP for D^{MS}	
(FP-type modification for D^{MS}, applied here for colour mixtures ($\Gamma = 1$).)	$D^{\text{MS}} = D^{\text{MS}}_{\text{MD}} + \frac{K_H}{\Gamma}\frac{\xi k_B T}{6\pi\eta L}$
YH-like for κ	
(Conductivity correction for colour mixtures, inspired by Jamali et al. [10].)	$\kappa = \kappa_{\text{MD}} + \frac{1}{36}\frac{\xi e^2 \rho}{\pi\eta L}$
FP for κ	
(FP-type conductivity correction with reduced hydrodynamic effects.)	$\kappa = \kappa_{\text{MD}} + \frac{K_H}{36}\frac{\xi e^2 \rho}{\pi\eta L}$

compared in Figure 1. In Figure 1(a) (high density), two regimes are evident for the viscosities of the system at $\rho = 0.85$. For simulation boxes larger than $N = 512$ ($L^{-1} \lesssim 0.12$) the viscosity is almost constant at $\eta_{\text{MD}} \approx 2.26$. Smaller simulation boxes show a pronounced oscillation, a feature previously reported by Kim et al. [15] and traced to configurational (virial–virial) contributions to the stress autocorrelation function. Our computed viscosities differ by less than 2% from those reported by Kim et al. [15]. The plateau at large N corroborates the conclusion of Yeh and Hummer [9] that the viscosity of a liquid is independent of system size. The data in Figure 1(b) (intermediate density) follow a straight line (dashed red), again consistent with Kim et al. [15]. Linear extrapolation to $L^{-1} \to 0$ yields $\eta \approx 0.399$, only 5% larger than the value obtained for the smallest simulation box. At low density, the viscosity changes non-linearly with system size (Figure 1(c)). Kim et al. showed that in this regime, the kinetic part of the stress–stress autocorrelation function dominates, leading to the finite-size scaling relation

$$\eta_{\text{MD}} = \eta + \frac{A}{L} + \frac{B}{L^3}, \tag{23}$$

where A and B are empirical constants and η is the viscosity in the thermodynamic limit [15]. Fitting Equation (23) to the computed viscosities at $\rho = 0.05$ (green symbols) produces the green dashed curve in Figure 1(c), which matches the data almost exactly and confirms that the viscosity is dominated by the kinetic contribution. The best-fit parameters are $\eta \approx 0.176$, $A = -0.019$, and $B = -5.9$. Note that Kim et al. [15] applied Equation (23) only to the kinetic contribution of the stress tensor to the viscosity. Finally, we compared the viscosity in the thermodynamic-limit obtained using the fit function in Equation (23) to the viscosity of an ideal-gas using the expression [34, 35],

$$\eta_{\text{id}} = \left(\frac{5}{16}\right)\frac{1}{d^2}\sqrt{\frac{mk_BT}{\pi}} \tag{24}$$

where d is effective molecular diameter taken as σ, $k_BT = 1$, and mass $m = 1$. Evaluating the above expression yields $\eta_{\text{id}} = 0.176$, in excellent agreement with η obtained from the fit in Equation (23). Note that the ideal gas viscosity in Equation (24) is independent of the density ρ. Overall, our viscosities match published data to within 2% for $\rho = 0.05$ and 0.45, and the observed finite-size effects follow the mechanisms proposed in the literature.

3.2. Self-diffusivities

We next focus on finite-size effects of self-diffusivities shown in Figure 2. At $\rho = 0.85$ the MD self-diffusivities in Figure 2(a) vary linearly with the inverse of the length of the simulation box (blue dashed line). Extrapolating this line to $L^{-1} \to 0$ yields $D^{\text{self}} \approx 0.07$. Applying the YH correction (Equation (6)) to $D^{\text{self}}_{\text{MD}}$ at each system size flattens the curve. The corrected values cluster around a constant mean (horizontal dashed line) that matches the extrapolated limit to within 0.1%. This shows that the YH correction removes finite-size effects exactly as expected for a dense liquid.

Adding Fushiki's hydrodynamic factor K_H to the correction (Equation (7)) makes virtually no difference, as in Figure 2(a) the cross markers lie almost exactly atop the plus symbols. Here, $K_H \simeq 0.98$, further confirming that the system behaves like a liquid at $\rho = 0.85$. For the D^{self} term in the Fushiki correction (Equation (7)), we use the value of the linear fit extrapolated to $L^{-1} \to 0$. Figure 2(b) shows the MD computed self-diffusivities at $\rho = 0.45$, together with various finite-size corrections. The uncorrected data follow a linear trend with the inverse of the simulation box length (red dashed line). We first applied the Yeh–Hummer term (Equation (6)) in two ways: (1) using the thermodynamic-limit viscosity η, obtained by extrapolating the line in Figure 1(b) to $L^{-1} \to 0$, and (2) using the size-dependent viscosities η_{MD}, obtained by inserting η and L into the same linear fit (Equation (23)). In both cases, the 'corrected' diffusivities still vary linearly with L^{-1}. These findings imply

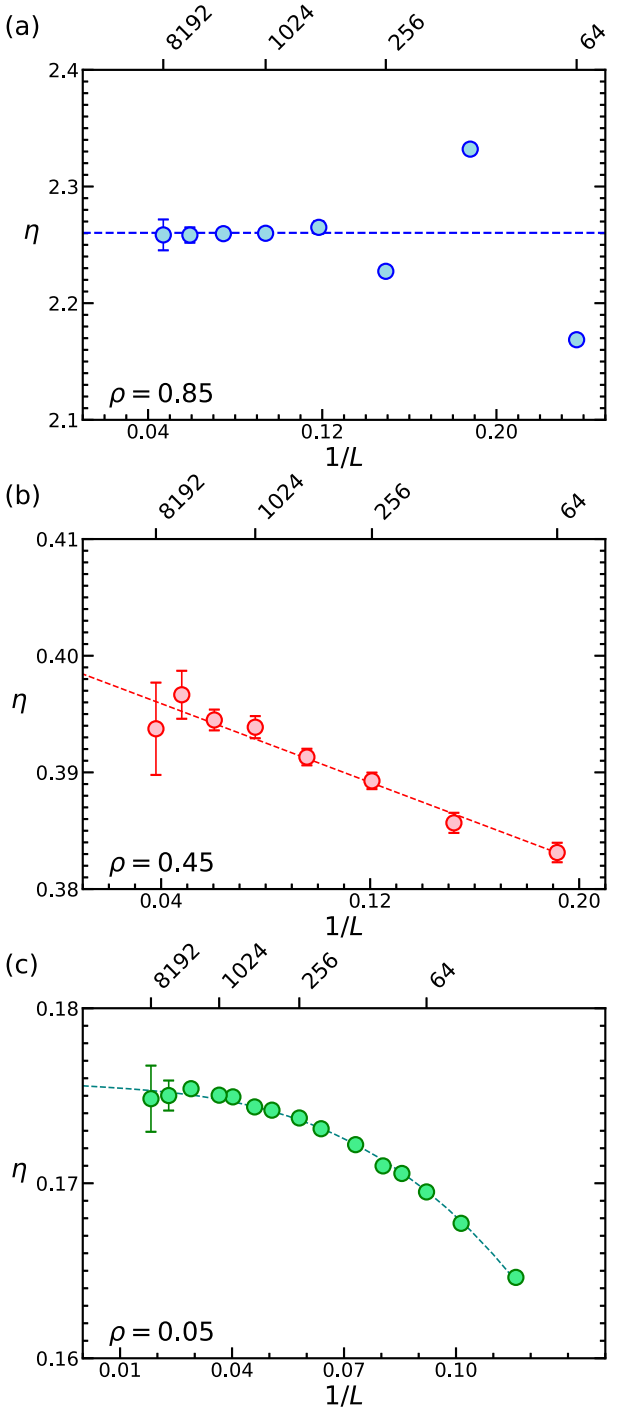

Figure 1. Finite-size effects for viscosities of single component systems. (a) $\rho = 0.85$ (dense), (b) $\rho = 0.45$ (intermediate), and (c) $\rho = 0.05$ (dilute). The dashed line in (a) represents the average MD computed viscosities for system sizes $N = 512$–8192. In (b) the dashed line is a linear fit to MD viscosities for $N = 64$–8192. Panel (c) shows MD viscosities fitted to Equation (23) (dashed line).

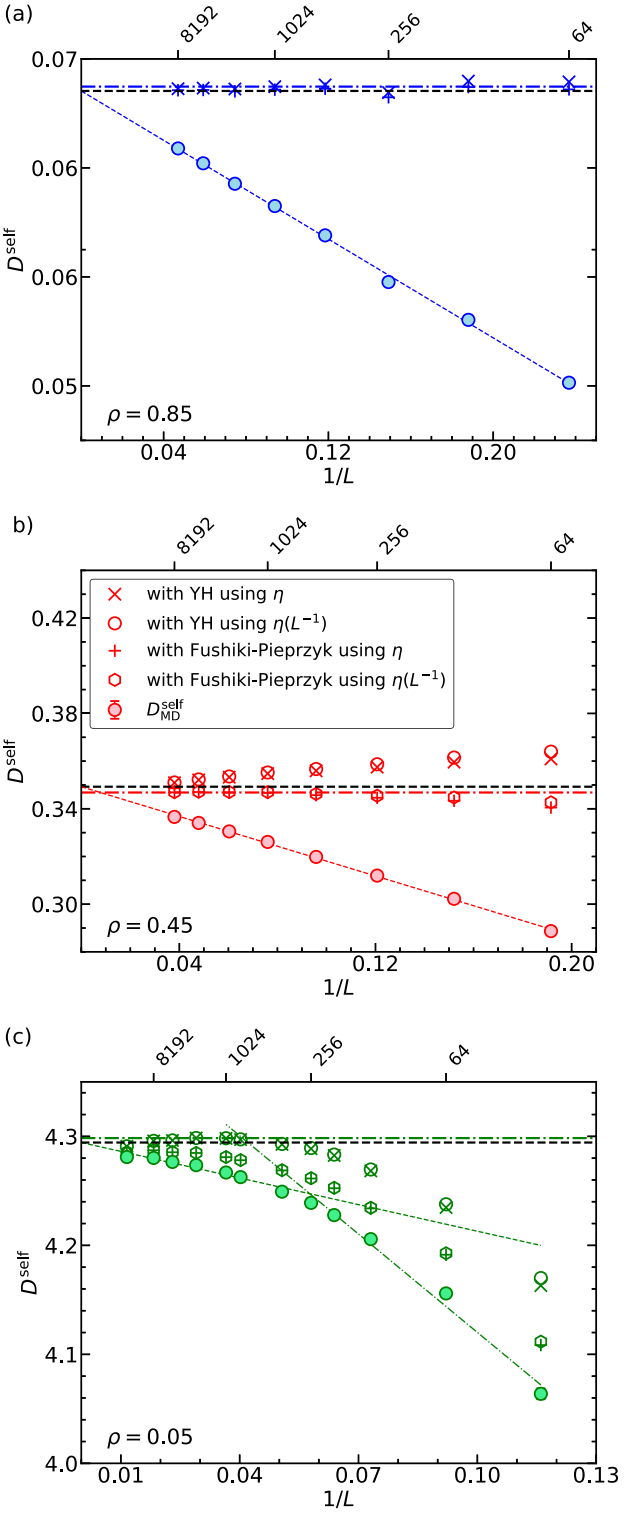

Figure 2. Finite-size effects of self-diffusivity D^{self} for single-component fluids: (a) dense ($\rho = 0.85$), (b) intermediate ($\rho = 0.45$), and (c) dilute ($\rho = 0.05$). Raw MD values (D^{self}_{MD}) are corrected using the Yeh–Hummer (YH) relation (Equation (6)) with either thermodynamic-limit or size-dependent viscosities, as well as the FP-modified YH form (Equation (7)). Dashed lines denote linear fits to the MD data, horizontal dashed lines indicate thermodynamic-limit extrapolations ($L^{-1} \to 0$), and dash-dotted lines mark mean corrected values (in panel (c), averaged over $N \geq 256$).

that the single $1/L$ term in the YH equation, appropriate for liquids, is not valid at $\rho = 0.45$. The system at $\rho = 0.45$ behaves more like a dense gas and likely requires higher-order corrections, similar to the viscosities at $\rho =$

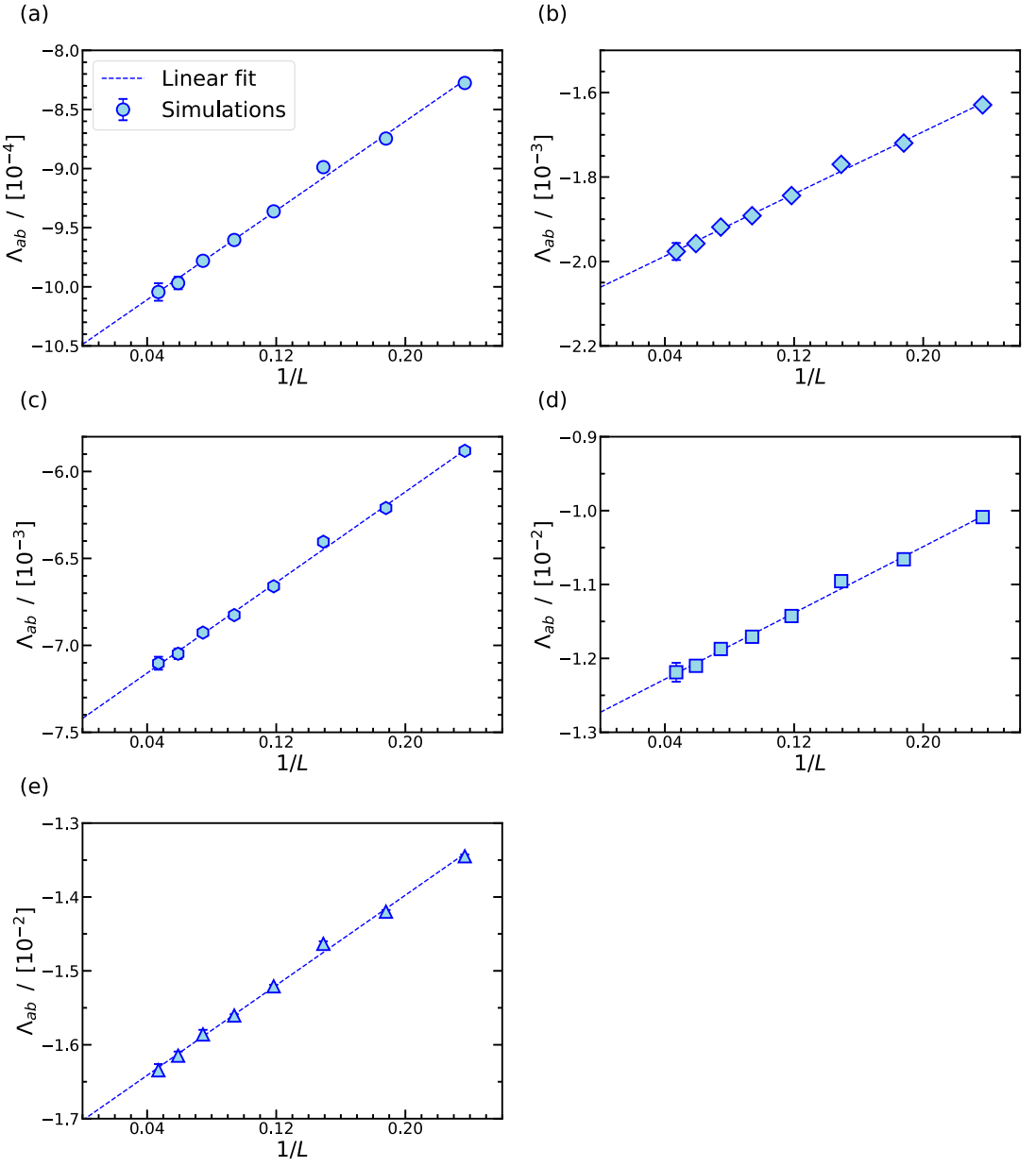

Figure 3. Finite-size effects of Onsager coefficients for an *AB* colour mixture at $\rho = 0.85$. Figures (a)–(e) display the finite-size effects on the Onsager coefficients for colour mixtures with mole fractions $x_A = 1/64, 1/32, 1/8, 1/4$, and 1/2 (with $x_A = 1 - x_B$), respectively. All dashed lines in figures (a)–(e) are linear fits to the MD computed Onsager coefficients.

0.45. To address this insufficiency in YH, we next apply Fushiki's hydrodynamic adjustment factor $K_H \simeq 0.54$ through the modified relation (Equation (7)). For the D^{self} term in the Fushiki correction (Equation (7)), we use the value of the linear fit extrapolated to $L^{-1} \to 0$. Whether η or η_{MD} is used, the corrected diffusivities become independent of system-size, in line with the observations for the hard-sphere systems of Pieprzyk et al. [24]. Interestingly, substituting η with η_{MD} has only a minor influence on the final values of $D^{\text{self}}_{\text{MD}}$ for the standard corrections and the Fushiki-modified corrections.

Unlike the cases at $\rho = 0.45$ and 0.85, the self-diffusivities in Figure 2(c) display two size regimes, captured by two separate linear fits: one for $32 \leq N < 256$ and another for $256 \leq N \leq 32{,}768$. Applying the Yeh–Hummer term (Equation (6)) yields an unexpected and non-trivial pattern. For $N \geq 256$ the corrected diffusivities collapse onto a size-independent cluster, whereas for $32 \leq N < 256$ the 'corrected' viscosities still vary with L^{-1}. Thus, the YH equation succeeds only when $N \geq 256$, in contrast to $\rho = 0.45$, where it failed even at $N = 8192$. Using the size-dependent viscosities η_{MD}

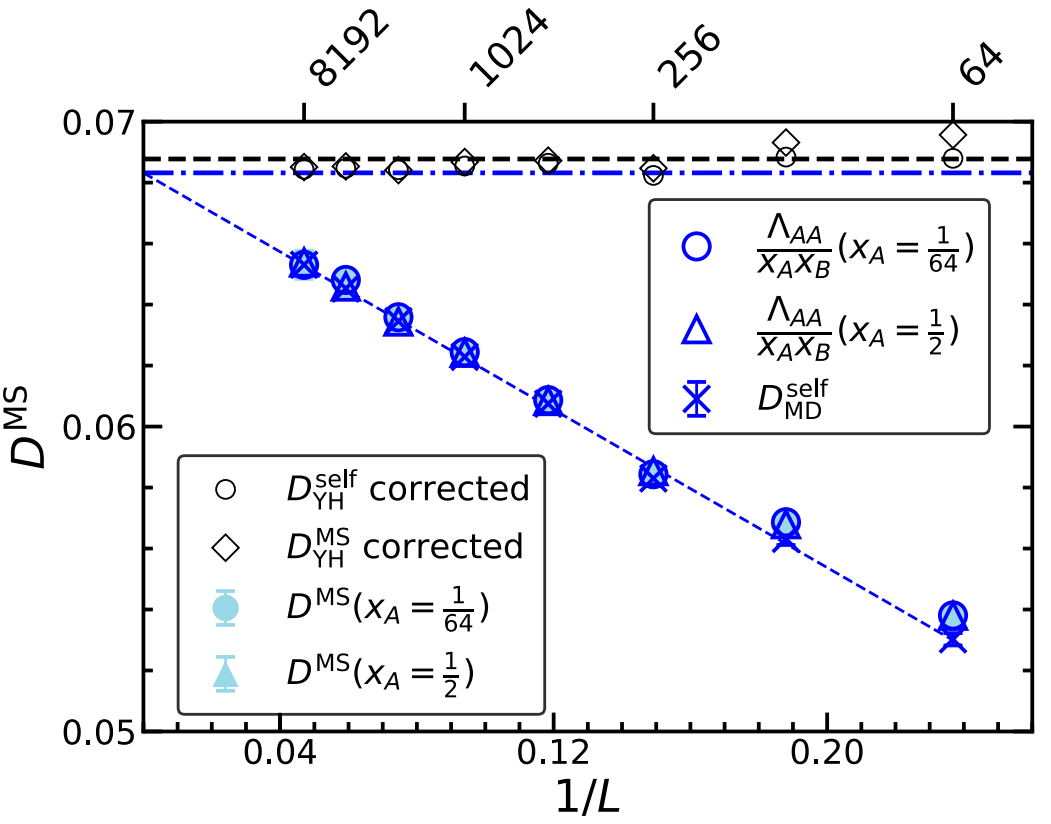

Figure 4. Finite-size effects of the MS diffusivity for an *AB* colour mixture at $\rho = 0.85$, evaluated using Equation (12). Results for D^{MS}_{MD} at mixture compositions of 1/64 and 1/2 are shown alongside the corresponding D^{self}_{MD} values at $\rho = 0.85$ (same as Figure 2(a)). The D^{MS}_{MD} obtained from Equation (12) are further compared with predictions from Equation (13), confirming the equivalence of the two approaches. The YH correction to the MS diffusivity (D^{MS}_{YH}) for $x_A = 1/64$ is calculated using Equation (14). The blue dashed line is the linear fit to the MD computed MS diffusivities. Extrapolating the linear fit to $L^{-1} \to 0$ gives the thermodynamic-limit MS-diffusivity, indicated by the (blue) dash-dotted horizontal line. The (black) horizontal dashed line marks the mean of the corrected MS-diffusivity.

(from Equation (23)) instead of the extrapolated thermodynamic value η has almost no effect on the finite-size corrections to D^{self}.

Applying Fushiki's factor $K_H = 0.29$ in Equation (7), with D^{self} taken from the linear fit for $256 \leq N \leq 32{,}768$, lowers the corrected D^{self}_{MD} relative to the standard YH term (Equation (6)). The adjusted values (green hexagons in Figure 2(c)) still vary linearly with L^{-1} and approach the YH plateau only at very large sizes ($N \gtrsim 32{,}768$), echoing the trend at $\rho = 0.45$ in Figure 2(b). Replacing η with η_{MD} leaves the result essentially unchanged. As a final consistency check, we compared our dilute-limit self-diffusivity with the ideal-gas prediction. Kinetic theory predicts [34, 35]

$$D^{self}_{id} = \frac{3}{8}\frac{1}{\rho\pi d^2}\sqrt{\frac{\pi k_B T}{m}} = \frac{3}{8}\frac{1}{\sqrt{\pi}\rho}, \qquad (25)$$

where we set $d = \sigma = 1, m = 1$, and $k_B T = 1$. Substituting $\rho = 0.05$ yields $D^{self}_{id} = 4.23$, very close to the value 4.21 obtained from the extrapolation in Figure 2(c). This agreement confirms the correctness of our calculations in the dilute limit.

Although a similar two-regime behaviour was noted by Pieprzyk et al. [24], the accompanying non-trivial finite-size corrections were not explored by these authors. Even in the hard-sphere study of Pieprzyk et al. [24], the lowest density examined was $\rho = 0.2$, where $K_H \approx 0.5$. Here, we probe much more dilute systems with $K_H \approx 0.29$. Evidently, hydrodynamic corrections become non-trivial at such low densities effective for some box sizes, ineffective for others. Thus, a more refined treatment is needed. One possibility is to introduce an additional L^{-3} term, analogous to the L^{-3} contribution in Equation (23) proposed by Kim et al. [15]. A detailed investigation of this option is left for future work.

3.3. Onsager coefficients

In the dense regime (Figure 3(a–e)) the Onsager coefficients Λ_{AB} for all five mole fractions of component A, x_A, decrease linearly with L^{-1}. The negative values of

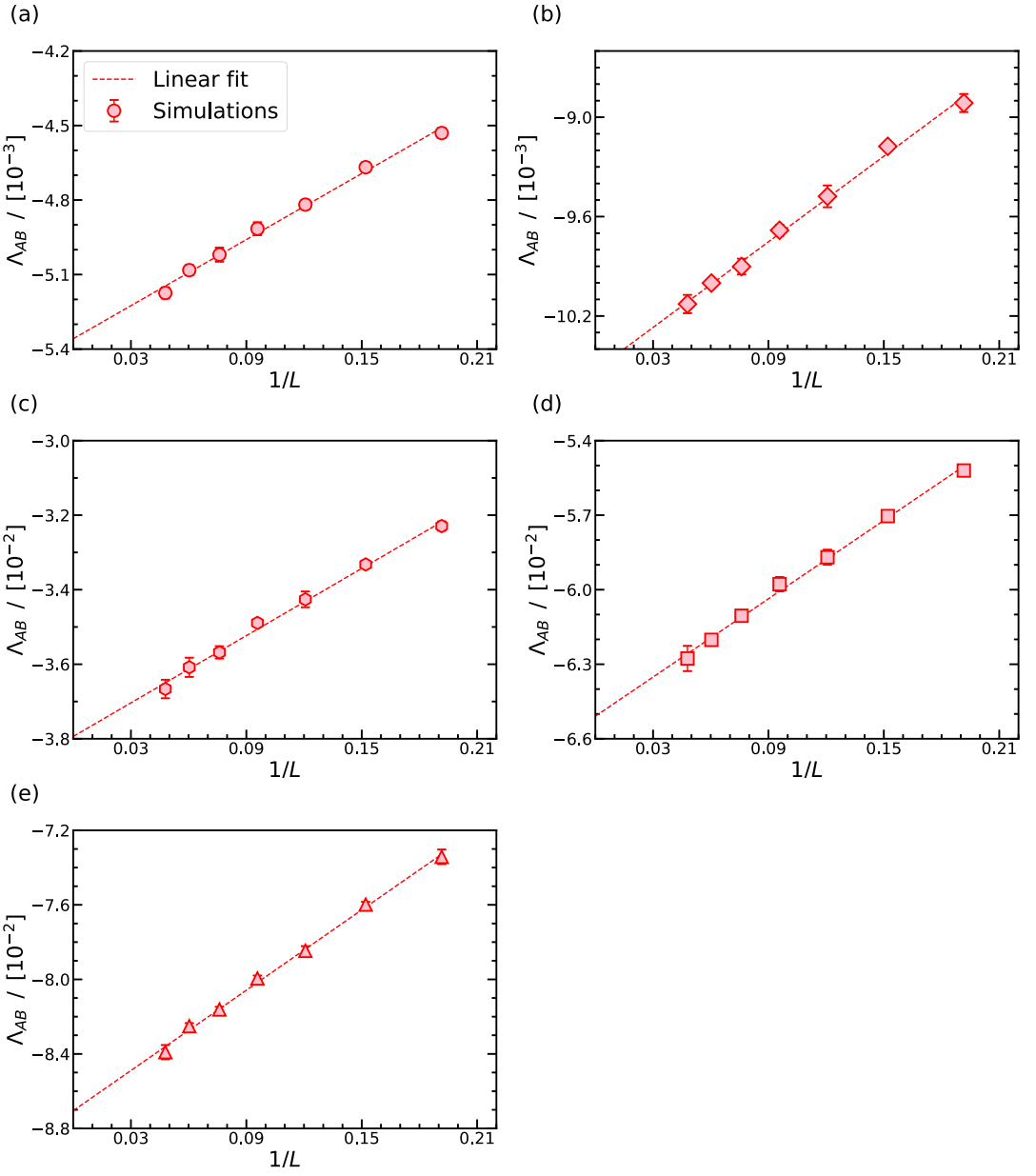

Figure 5. Finite-size effects of Onsager coefficients for an *AB* colour mixture at $\rho = 0.45$. Figures (a)–(e) display the finite-size effects on the Onsager coefficients for colour mixtures with mole fractions $x_A = 1/64, 1/32, 1/8, 1/4$, and $1/2$ (with $x_A = 1 - x_B$), respectively. All dashed lines in figures (a)–(e) are linear fits to the MD computed Onsager coefficients.

Λ_{AB} implies anticorrelated displacements that grow in magnitude with x_A, reaching a maximum at $x_A = 1/2$. Combining the Onsager coefficients using Equation (12) yields MS diffusivities $D^{\mathrm{MS}}_{\mathrm{MD}}$ shown in Figure 4. $D^{\mathrm{MS}}_{\mathrm{MD}}$ also varies linearly with L^{-1}. Because the colour mixture is symmetric, the finite-size correction reduces to the standard YH equation (Equation (14)). Applying this correction yields $D^{\mathrm{MS}} \simeq 0.068$, essentially the same as the self-diffusivity D^{self}. This match is expected, as in a colour mixture the colour label does not alter the dynamics. For each system size, we confirm that $\Lambda_{AA} = \Lambda_{BB} = -\Lambda_{AB}$ (Equation (11)). As an extra check, Figure 4 shows the overlap of $\Lambda_{AA}/(x_A x_B)$ (unfilled symbols) and $D^{\mathrm{MS}}_{\mathrm{MD}}$ at the two extreme compositions $x_A = 1/64$ and $x_A = 1/2$. At $\rho = 0.85$, the Onsager coefficients and the MS-diffusivities show finite-size effects that scale linearly with L^{-1} and the standard YH correction (Equation (14)) mitigates this effect.

We now examine the Onsager coefficients Λ_{AB} at $\rho = 0.45$ in Figure 5(a–e). For each mole fraction, Λ_{AB} scales linearly with L^{-1} (Figure 5(a–e)), becoming more negative as size of the simulation box increases. The magnitude increases with x_A, as larger subgroups of particles collectively move larger distances than smaller

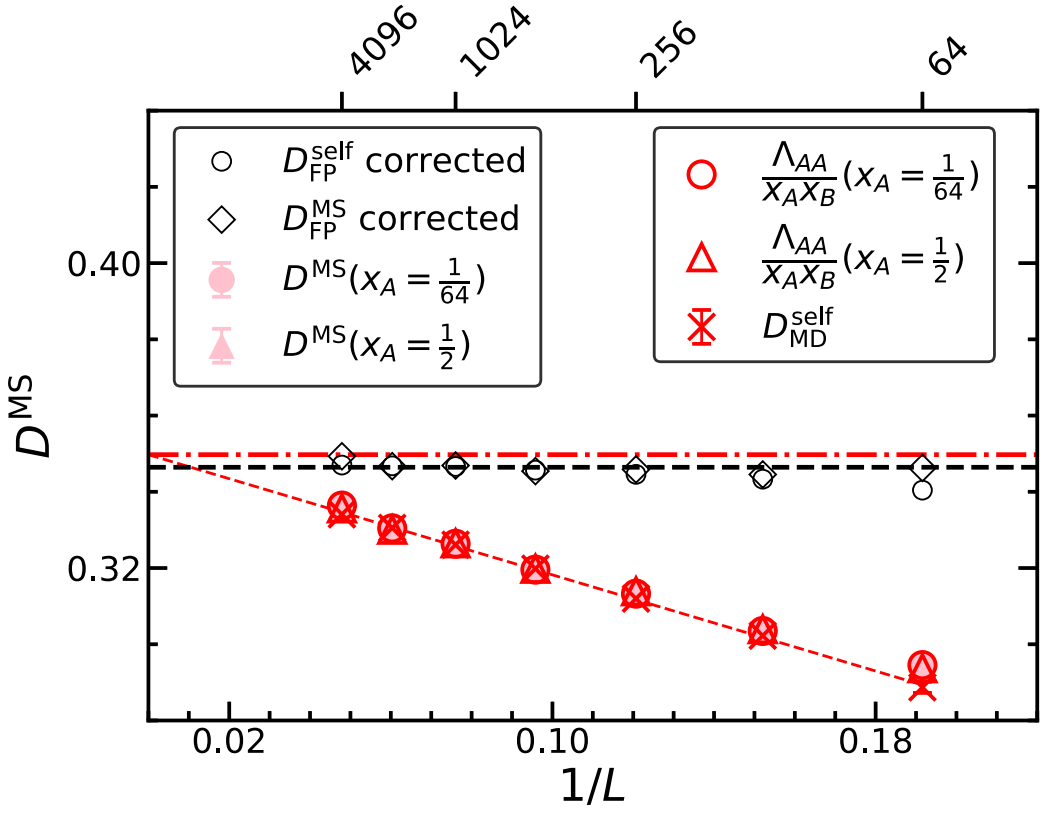

Figure 6. Finite-size effects of the MS diffusivity for an *AB* colour mixture at $\rho = 0.45$, evaluated using Equation (12). Results for $D^{\mathrm{MS}}_{\mathrm{MD}}$ at mixture compositions of 1/64 and 1/2 are shown alongside the corresponding $D^{\mathrm{self}}_{\mathrm{MD}}$ values at $\rho = 0.45$ (same as Figure 2(b)). The $D^{\mathrm{MS}}_{\mathrm{MD}}$ obtained from Equation (12) are further compared with predictions from Equation (13), confirming the equivalence of the two approaches. The YH correction to the MS diffusivity ($D^{\mathrm{MS}}_{\mathrm{YH}}$) for $x_A = 1/64$ is calculated using Equation (14). The red dashed line is the linear fit to the MD computed MS diffusivities. Extrapolating the linear fit to $L^{-1} \to 0$ gives the thermodynamic-limit MS-diffusivity, indicated by the (red) dash-dotted horizontal line. The (black) horizontal dashed line marks the mean of the corrected MS-diffusivity.

subgroups. Using these coefficients in Equation (12) yields the MS diffusivity, which also varies linearly with L^{-1} (Figure 6). As expected for colour mixtures, the resulting $D^{\mathrm{MS}}_{\mathrm{MD}}$ matches the self-diffusivity of each system. The two extreme compositions ($x_A = 1/64$ and $x_A = 1/2$) are shown explicitly in Figure 6. Because $D^{\mathrm{MS}}_{\mathrm{MD}}$ and the self-diffusivity have identical magnitudes, any finite-size correction that is valid for the self-diffusivity should apply directly to the MD diffusivity. At this density the standard YH term fails, while the Fushiki factor in Equation (7) mitigates the finite-size effects (see also the discussion on finite-size corrections for self-diffusivities at $\rho = 0.45$). It remains to be seen how these corrections perform for binary mixtures whose components have different interactions and dynamics.

The Onsager coefficients Λ_{AB} and MS diffusivities at $\rho = 0.05$ are shown in Figure 7(a–e). Because each Onsager coefficient is a cross-correlation, simulations beyond $N = 1024$ become prohibitively expensive, and the long convergence time ($t \approx 1000$ vs. $t = 50$ at $\rho = 0.85$ and $t = 1000$ at $\rho = 0.05$, Table 2) further amplifies the computational cost. Similar to $\rho = 0.85$ and $\rho = 0.45$, the Onsager coefficient Λ_{AB} varies linearly with L^{-1} for each mole fraction in Figure 7(a–e). The resulting system size dependence of the MS diffusivities, obtained by combining the Onsager coefficients of Figure 7(a–e), is shown in Figure 8 for $x_A = 1/64$ and 1/2. For comparison, the corresponding self-diffusivities of Figure 2(c) are also included. An interesting trend emerges, the MS and self-diffusivities agree very well for $N \geq 256$, but deviate sharply for $N < 256$. Although it is known that D^{self} and D^{MS} for a colour mixture should coincide in the thermodynamic limit, our results demonstrate that this equivalence breaks down at small system sizes in the dilute regime due to different finite-size effects. This represents a noteworthy finding that merits further investigation.

3.4. Electrical conductivities

The finite-size effects on electrical conductivity κ are shown in Figure 9(a–c). At $\rho = 0.85$ (Figure 9(a)), κ

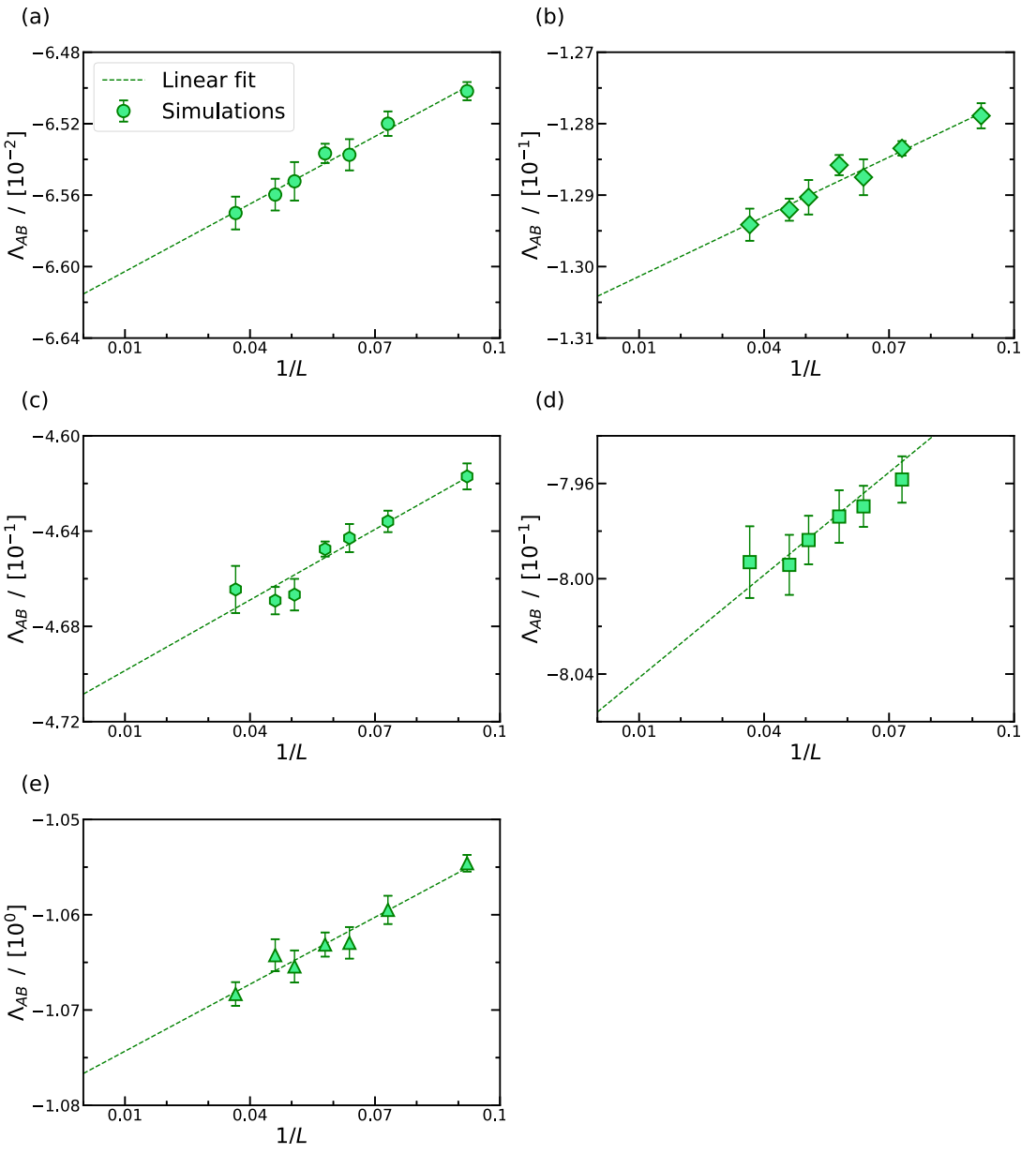

Figure 7. Finite-size effects of Onsager coefficients for an *AB* colour mixture at $\rho = 0.05$. Figures (a)–(e) show the finite-size dependence of Onsager coefficients for different mole fractions of component *A* (x_A) in the colour mixture. All dashed lines in panels (a)–(e) are linear fits to the MD-computed Onsager coefficients.

increases linearly with length of the simulation box for $N = 64$–8192, as indicated by the dashed fit line. Applying the YH correction from Equation (21) produces corrected values (blue crosses) that are nearly independent of system size. The mean corrected conductivity differs only about 2% from the thermodynamic limit value obtained by extrapolating the fit to $L^{-1} \to 0$. We attribute this to the relatively short simulation times. We expect longer runs will reduce this difference. Overall, the YH correction effectively mitigates finite-size effects at $\rho = 0.85$.

At $\rho = 0.45$ (Figure 9(b)), κ again scales linearly with the length of the simulation box, as shown by the dashed fit. Applying the standard YH correction from Equation (21) still leaves a size dependence, indicating that the YH form is insufficient. Inspired by the modified YH approach for D^{self} by Fushiki [23] and Pieprzyk [24] (see Equation (7) and Figure 2(b)), we multiply the YH term by the non-dimensional hydrodynamic factor $K_H = \nu/(\nu + D^{\text{self}})$ (with $K_H = 0.54$ at $\rho = 0.45$). This modified correction removes the finite-size trend, and the mean corrected conductivity deviates by only about 2% from the thermodynamic-limit value obtained by extrapolation. Although the agreement between the modified YH-corrected conductivity and the thermodynamic-limit value (from linear extrapolation to

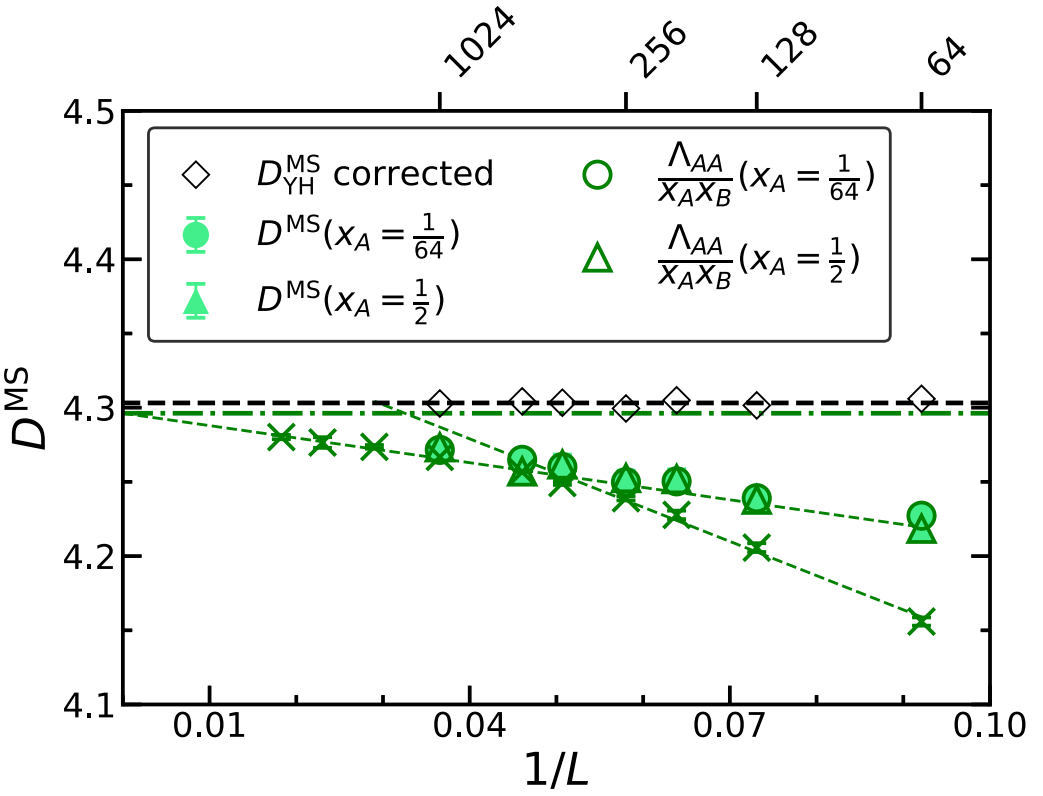

Figure 8. Finite-size effects of the MS diffusivity for an *AB* colour mixture at $\rho = 0.05$, evaluated using Equation (12). Results for D^{MS}_{MD} at mixture compositions of 1/64 and 1/2 are shown alongside the corresponding D^{self}_{MD} values at $\rho = 0.05$. The D^{MS}_{MD} obtained from Equation (12) are further compared with predictions from Equation (13), confirming the equivalence of the two approaches. The two green dashed lines represent linear fits to the MD self-diffusivities for $N < 256$ and $N \geq 256$, respectively (same as Figure 2(c)). Extrapolating the linear fit to $L^{-1} \to 0$ gives the thermodynamic-limit MS-diffusivity, indicated by the (green) dash-dotted horizontal line. The (black) horizontal dashed line marks the mean of the corrected MS-diffusivity.

$L^{-1} \to 0$) is within about 2%, this improvement underscores that hydrodynamic assumptions become questionable at intermediate densities and must be addressed in future corrections.

The finite-size effects on electrical conductivity κ at $\rho = 0.05$ are shown in Figure 9(c). Here, κ increases nearly linearly with box length, as indicated by the green dashed-line fit, but the total variation is only about 2% from $N = 64$ to the value of κ at the thermodynamic limit ($L^{-1} \to 0$). In sharp contrast, the variation reaches 15% at $\rho = 0.45$ (Figure 9(b)) and 20% at $\rho = 0.85$ (Figure 9(a)). Surprisingly, applying the standard YH correction for conductivity (Equation (21)) essentially removes the size dependence: the mean corrected κ matches the thermodynamic-limit value obtained by extrapolating the linear fit in Figure 9(c) to $L^{-1} \to 0$. This robust performance of the standard YH mirrors the behaviour seen for self-diffusivities at $\rho = 0.05$, where the standard YH correction for D^{self} (Equation (6)) worked well for $N \geq 192$ (Figure 2(c)). Although the hydrodynamic assumptions underlying these corrections are most questionable at low densities, their success here suggests further investigation into finite-size effects is warranted.

4. Conclusions and outlook

We have quantified finite-size effects on shear viscosity, self-diffusivity, Onsager coefficients (and derived MS diffusivities), and electrical conductivity κ at reduced densities $\rho = 0.05$, 0.45, and 0.85 via MD simulations of WCA particles. At $\rho = 0.85$, shear viscosity is constant for $N \geq 512$ and shows minor oscillations below $N = 512$, reflecting dominant contributions from the configurational stress [15]. At $\rho = 0.45$, viscosity scales linearly with $1/L$, as previously reported [15], while at $\rho = 0.05$ we observe, for the first time, an additional $1/L^3$ term arising from kinetic contributions superimposed on the $1/L$ scaling. The standard Yeh–Hummer correction removes finite-size effects of the self-diffusivity at $\rho = 0.85$, but fails at intermediate densities, where adding the Fushiki–Pieprzyk hydrodynamic factor K_H restores agreement. At $\rho = 0.05$, neither corrections fully mitigates the finite-size effects for $N < 192$, suggesting that an

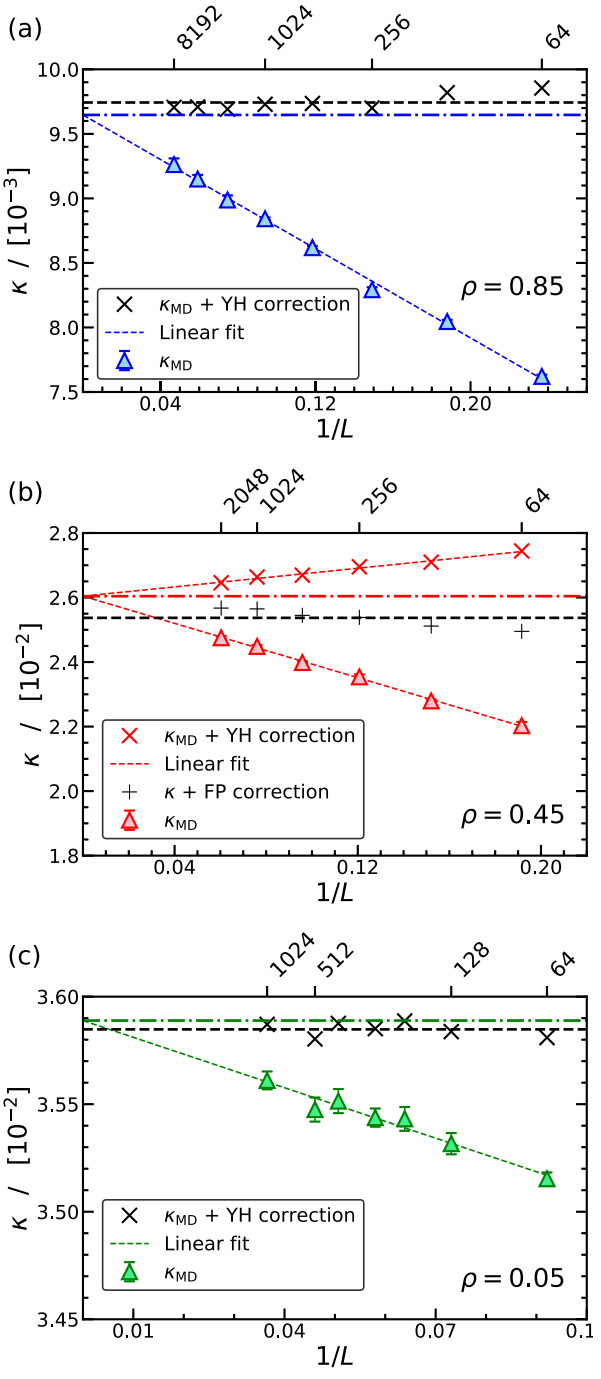

Figure 9. Finite-size effects of electrical conductivity κ for *AB* molten-salt systems at $x_A = x_B = 1/2$: (a) $\rho = 0.85$, (b) $\rho = 0.45$, and (c) $\rho = 0.05$. The standard YH correction (Equation (21)) and the FP-modified form (Equation (22)) are applied to κ_{MD}. In (a), (b), and (c), dashed lines denote linear fits to MD data, dash–dot lines mark the extrapolated thermodynamic-limit values ($L^{-1} \to 0$), and black dashed lines indicate the mean corrected κ.

additional correction $1/L^3$ may be needed. For $N > 192$ the finite-size effects at $\rho = 0.05$ can be corrected using the standard YH correction. Onsager coefficients of *AB* colour mixtures scale linearly with $1/L$, except in the most dilute gas-like cases ($x_A = 1/64, 1/32, 1/8$ at $\rho = 0.05$). MS diffusivities derived from the Onsager coefficients agree with self-diffusivities for all densities, and the same finite-size corrections apply to both. For electrical conductivities in molten-salt colour mixtures, the standard YH correction for κ (Equation (21)) successfully removes finite-size effects at $\rho = 0.85$ and unexpectedly at $\rho = 0.05$. At $\rho = 0.45$, the modified YH form (with K_H) suffices. These results reveal a non-hydrodynamic regime at intermediate densities. Overall, our findings highlight the necessity of addressing finite-size effects in MD studies computing transport properties of dense-gas or gas-like systems (intermediate and low densities). While the WCA particle model offers computational efficiency and allows a systematic assessment of finite-size effects, it lacks direct chemical specificity.

To provide practical guidance, Table 5 summarises the recommended correction schemes, the minimum system sizes, and their accuracy in densities. This overview allows readers to identify when finite-size artefacts can be reliably corrected, when direct extrapolation is required, and when performing simulations is essential. Future work could theoretically investigate the behaviour of finite-size corrections in non-hydrodynamic regimes, thereby improving predictions of transport properties of gas-like mixtures.

Table 5. Summary of recommended corrections and minimum system sizes across densities. Here, YH = Yeh–Hummer, FP = Fushiki–Pieprzyk, N = number of particles. Accuracy is quantified by extrapolating the relevant property to the infinite system-size limit ($L^{-1} \to 0$), which serves as the reference. The relative deviation of the finite-size corrected property from this reference value is then reported as the accuracy, reflecting the confidence with which the infinite system-size property can be predicted. For properties where no correction is available, a linear ($\rho = 0.45$) or cubic extrapolation ($\rho = 0.05$) with $1/L$ is required to obtain the value of property at the thermodynamic limit. For $\rho = 0.85$, the viscosity is constant for $N \geq 512$, but exhibits oscillatory behaviour for $N < 512$, where no finite-size corrections are available.

ρ	Property	Correction	Min. N	Accuracy [%]
0.85	η	–	64	Oscillatory ($N < 512$)
	D^{self}	YH	64	0.3
	D^{MS}	YH-like	64	0.3
	κ	YH-like	64	1
0.45	η	–	64	Extrapolate
	D^{self}	FP	64	0.7
	D^{MS}	FP-like	64	0.7
	κ	FP-like	64	2.6
0.05	η	–	64	Extrapolate
	D^{self}	YH	256	0.1
	D^{MS}	YH-like	64	0.2
	κ	YH-like	64	0.1

Acknowledgments

T.H.C. acknowledges the use of the Civil Engineering Department cluster at Delft University of Technology for the initial simulations.

Data availability statement

Data is available from the authors at reasonable request.

Disclosure statement

No potential conflict of interest was reported by the author(s).

Funding

No funding was reported for this research.

ORCID

Othonas A. Moultos http://orcid.org/0000-0001-7477-9684
Thijs J. H. Vlugt http://orcid.org/0000-0003-3059-8712
Thejas Hulikal Chakrapani https://orcid.org/0000-0002-8182-345X

References

[1] R.B. Bird, W.E. Stewart and E.N. Lightfoot, *Transport Phenomena*, 2nd ed. (John Wiley & Sons, New York, 2007).
[2] D.B. Ingham and I. Pop, *Transport Phenomena in Porous Media III*, 1st ed., 3 vols. (Elsevier, Oxford, 2005).
[3] A. Hassanpouryouzband, E. Joonaki, K. Edlmann, N. Heinemann and J. Yang, Sci. Data **7**, 222 (2020). doi:10.1038/s41597-020-0568-6
[4] R.L. Fournier, *Basic Transport Phenomena in Biomedical Engineering*, 4th ed. (CRC press, Boca Raton, 2017).
[5] D. Frenkel and B. Smit, *Understanding Molecular Simulation, from Algorithms to Applications*, 3rd ed. (Elsevier Science, Oxford, 2023).
[6] M.P. Allen and D. Tildesley, *Computer Simulation of Liquids*, 2nd ed. (Oxford University Press, Oxford, 2017).
[7] E.J. Maginn, R.A. Messerly, D.J. Carlson, D.R. Roe and J.R. Elliot, Living J. Comp. Mol. Sci. **1**, 6324–6324 (2019).
[8] B. Dünweg and K. Kremer, J. Chem. Phys. **99**, 6983–6997 (1993). doi:10.1063/1.465445
[9] I.C. Yeh and G. Hummer, J. Phys. Chem. B **108**, 15873–15879 (2004). doi:10.1021/jp0477147
[10] S.H. Jamali, L. Wolff, T.M. Becker, A. Bardow, T.J.H. Vlugt and O.A. Moultos, J. Chem. Theory Comput. **14**, 2667–2677 (2018). doi:10.1021/acs.jctc.8b00170
[11] S.H. Jamali, A. Bardow, T.J.H. Vlugt and O.A. Moultos, J. Chem. Theory Comput. **16**, 3799–3806 (2020). doi:10.1021/acs.jctc.0c00268
[12] A.T. Celebi, S.H. Jamali, A. Bardow, T.J.H. Vlugt and O.A. Moultos, Mol. Sim. **47**, 831–845 (2021). doi:10.1080/08927022.2020.1810685
[13] T. Hulikal Chakrapani, H. Hajibeygi, O.A. Moultos and T.J.H. Vlugt, Ind. Eng. Chem. Res. **63**, 10456–10481 (2024). doi:10.1021/acs.iecr.4c01078
[14] J.D. Weeks, D. Chandler and H.C. Andersen, J. Chem. Phys. **54**, 5237–5247 (1971). doi:10.1063/1.1674820
[15] K.S. Kim, C. Kim, G.E. Karniadakis, E.K. Lee and J.J. Kozak, J. Chem. Phys. **151**,104101(2019). doi:10.1063/1.5113751
[16] D.M. Heyes, M.J. Cass, J.G. Powles and W.A.B. Evans, J. Phys. Chem. B **111**, 1455–1464 (2007). doi:10.1021/jp067373s
[17] L. Verlet, Phys. Rev. **159**, 98–103 (1967). doi:10.1103/PhysRev.159.98
[18] P.J. Daivis and D.J. Evans, J. Chem. Phys. **100**, 541–547 (1994). doi:10.1063/1.466970
[19] J. Ramírez, S.K. Sukumaran, B. Vorselaars and A.E. Likhtman, J. Chem. Phys. **133**,154103(2010). doi:10.1063/1.3491098
[20] O.A. Moultos, Y. Zhang, I.N. Tsimpanogiannis, I.G. Economou and E.J. Maginn, J. Chem. Phys. **145**, 074109 (2016). doi:10.1063/1.4960776
[21] S.H. Jamali, R. Hartkamp, C. Bardas, J. Söhl, T.J.H. Vlugt and O.A. Moultos, J. Chem. Theory and Comput. **14**, 5959–5968 (2018). doi:10.1021/acs.jctc.8b00625
[22] J. Busch and D. Paschek, J. Phys. Chem. B **127**, 7983–7987 (2023). doi:10.1021/acs.jpcb.3c04492
[23] M. Fushiki, Phys. Rev. E **68**,021203(2003). doi:10.1103/PhysRevE.68.021203
[24] S. Pieprzyk, M.N. Bannerman, A.C. Brańka, M. Chudak and D.M. Heyes, Phys. Chem. Chem. Phys. **21**, 6886–6899 (2019). doi:10.1039/C9CP00903E
[25] R. Taylor and R. Krishna, *Multicomponent Mass Transfer*, 1st ed. (John Wiley & Sons, New York, 1993).
[26] R. Krishna and J.A. Wesselingh, Chem. Eng. Sci. **52**, 861–911 (1997). doi:10.1016/S0009-2509(96)00458-7
[27] X. Liu, A. Bardow and T.J.H. Vlugt, Ind. Eng. Chem. Res. **50**, 4776–4782 (2011). doi:10.1021/ie102515w
[28] X. Liu, S.K. Schnell, J.M. Simon, D. Bedeaux, S. Kjelstrup, A. Bardow and T.J.H. Vlugt, J. Phys. Chem. B **115**, 12921–12929 (2011). doi:10.1021/jp208360s
[29] T. Hulikal Chakrapani, H. Hajibeygi, O.A. Moultos and T.J.H. Vlugt, J. Chem. Theory Comput. **20**, 333–347 (2024). doi:10.1021/acs.jctc.3c01144
[30] R. Krishna and J.M. van Baten, Ind. Eng. Chem. Res. **44**, 6939–6947 (2005). doi:10.1021/ie050146c
[31] E.L. Cussler, *Diffusion: Mass Transfer in Fluid Systems*, 3rd ed. (Cambridge University press, Cambridge, 2009).
[32] S. Blazquez, J.L.F. Abascal, J. Lagerweij, P. Habibi, P. Dey, T.J.H. Vlugt, O.A. Moultos and C. Vega, J. Chem. Theory Comput. **19**, 5380–5393 (2023). doi:10.1021/acs.jctc.3c00562
[33] P. Habibi, J.R. Postma, J.T. Padding, P. Dey, T.J.H. Vlugt and O.A. Moultos, Ind. Eng. Chem. Res.**62**, 11992–12005 (2023). doi:10.1021/acs.iecr.3c01422
[34] S. Chapman and T.G. Cowling, *The Mathematical Theory of Non-uniform Gases: An Account of the Kinetic Theory of Viscosity, Thermal Conduction and Diffusion in Gases*, 3rd ed. (Cambridge University Press, Cambridge, 1970).
[35] D. Enskog, Kungl. Svenska Vetenskap. Handl. **63**, 1–44 (1922).